Pergamon

Chemical Engineering Science, Vol. 49, No. 17, pp. 3001–3014, 1994

0009–2509/94 $7.00 + 0.00

0009–2509(94)E0117–9

POINT DEFECTS IN CRYSTALLINE SILICON, THEIR MIGRATION AND THEIR RELATION TO THE AMORPHOUS PHASE

DIMITRIS MAROUDAS† and SOKRATES T. PANTELIDES
IBM Research Division, Thomas J. Watson Research Center, Yorktown Heights, NY 10598, U.S.A.

(*First received* 1 *September* 1993; *accepted in revised form* 16 *December* 1993)

Abstract—Vacancies and self-interstitials in silicon have been studied extensively both experimentally and theoretically and many of their properties have been established. We review briefly some of the recent results obtained by *ab initio* calculations and by atomistic simulations using empirical interatomic potentials. These results yield a comprehensive picture of defect structure, migration paths, and relative contributions to self-diffusion. We elucidate the details of the atomic migration process by analyzing one of the migration paths of the self-interstitial in terms of the lattice normal modes (phonons). Finally, we report new calculations to clarify further similarities between crystals containing large concentrations of point defects and amorphous silicon. In addition to a notable trend in the density of crystals containing increasingly higher self-interstitial concentrations, we find strong similarities in the vibrational and structural properties.

INTRODUCTION

Intrinsic point defects, such as vacancies and self-interstitials, are known to mediate mass transport in crystalline and polycrystalline solids. Therefore, they play a key role in determining many materials properties. In crystalline semiconductors, point defects mediate the diffusion of substitutional dopant impurities and, thus, ultimately control the electronic properties of the crystal (Fahey *et al.*, 1989). In polycrystals, point defects mediate self-diffusion and, thus, control diffusional creep (Herring, 1950). Furthermore, point defects mediate dislocation climb and, therefore, play a key role in controlling crystal plasticity (Balluffi and Granato, 1979).

Over the years, there has been considerable experimental and theoretical research seeking to unravel the structure of point defects, their migration paths, and their relative contributions to self-diffusion and impurity diffusion. In silicon, experimental data yielded conflicting evidence and caused intense debates, especially regarding the relative contributions of point defects to self-diffusion and substitutional dopant diffusion (Tan and Gösele, 1985; Fahey *et al.*, 1989). In the last ten years, theory has made significant advances using both first-principles calculations (Car *et al.*, 1984; Bar-Yam and Joannopoulos, 1984a, b, c; Pantelides, 1990, 1992; Blöchl *et al.*, 1993) and atomistic simulations based on empirical interatomic potentials (Batra *et al.*, 1987; Schober, 1989; Maroudas and Brown, 1993a, b). It has been established that both vacancies and self-interstitials in silicon are negative-U centers, which means that certain charge states are unstable exhibiting negative electron–electron correlation energy U and, thus, spontaneously decay into other charge states (Baraff *et al.*, 1979; Car *et al.*, 1984). It has been established that the self-interstitial exists in several stable configurations with comparable formation energies, giving rise to a multiplicity of migration paths (Car *et al.*, 1984). Some of these configurations are *simple*, e.g. an extra silicon atom occupying an interstitial site of tetrahedral symmetry with minimal lattice relaxation, whereas others are *interstitialcies*, i.e. configurations that involve substantial lattice relaxation making it impossible to single out the extra silicon atom. In recent work, it has been established that self-interstitials in the form of an interstitialcy dominate the self-diffusion process (Blöchl *et al.*, 1993).

In this paper, we will first review briefly the most recent theoretical results regarding vacancies and self-interstitials in silicon and their role in mediating self-diffusion. A set of complementary finite-temperature calculations from first principles (Blöchl *et al.*, 1993) and from an empirical interatomic potential (Maroudas and Brown, 1993a, b) yield a comprehensive picture. Furthermore, these results allow us to assess the validity of the quasi-harmonic approximation (Jacucci and Quirke, 1982) in computing vibrational entropies. Then, we focus our attention on a particular migration path for the self-interstitial, namely the simple path that passes through the tetrahedral and the hexagonal interstitial sites. We analyze the migration process in terms of lattice vibrations. In particular, we determine the phonon admixtures that correspond to adiabatic migration from the tetrahedral to a nearest-neighbor tetrahedral site through the hexagonal site.

†Permanent address: Department of Chemical and Nuclear Engineering, University of California, Santa Barbara, CA 93106, U.S.A.

In the remainder of the paper, we address another issue that has lately been raised in the literature: the possible relation between point defects in crystalline silicon with the structure and properties of the amorphous phase (Torres *et al.*, 1987; Schober, 1989; Maroudas and Brown, 1993a). It has often been noted that the relaxed self-interstitials constitute small amorphous regions (Seeger and Chik, 1968). Therefore, we have studied the structure and properties of crystalline silicon with an increasingly higher concentration of either vacancies or self-interstitials. We find that a crystal with a high concentration of self-interstitials has many structural properties similar to those of amorphous silicon.

Several empirical and semiempirical atomic models have been proposed for the computer simulation of silicon (Stillinger and Weber, 1985; Biswas and Hamann, 1985; Tersoff, 1986, 1988a, b; Baskes, 1987, 1992; Kaxiras and Pandey, 1988; Chelikowsky *et al.*, 1989). The atomic model for silicon used in this study is the interatomic potential developed by Stillinger and Weber (1985), which includes two-body attractive and repulsive interactions and three-body repulsive interactions (Stillinger and Weber, 1985). The Stillinger–Weber (SW) potential was chosen because it predicts successfully structural, formation, and migration properties of self-interstitials in bulk silicon (Batra *et al.*, 1987; Schober, 1989; Maroudas and Brown, 1993a, b) and, most importantly, because it reproduces very well the experimentally measured phonon dispersion curves for crystalline silicon (Broughton and Li, 1987). Furthermore, the SW potential gives an excellent prediction of the melting temperature of silicon (Broughton and Li, 1987) and satisfactory predictions of vacancy migration (Maroudas and Brown, 1993a), both of which are key properties for the study of point defects at high temperatures.

POINT DEFECTS AND SELF-DIFFUSION IN SILICON

A combination of experimental and theoretical investigations over many years has provided detailed information about the properties of point defects in silicon and relative contributions to self-diffusion. A key role in establishing these properties was played by theoretical calculations (Baraff *et al.*, 1979; Car *et al.*, 1984; Bar-Yam and Joannopoulos, 1984a, b, c; Schober, 1989) and especially by the more recent finite-temperature calculations both from first principles (Blöchl *et al.*, 1993) and from empirical interatomic potentials (Maroudas and Brown, 1993a, b). In this section we give a brief summary of the comprehensive picture that has emerged.

The vacancy (V) is by far the simplest point defect. Lattice relaxation reduces the symmetry of the defect in a manner that depends on the charge state. The symmetry-lowering relaxations are driven by the so-called Jahn–Teller effect, namely the fact that such relaxations split a partially occupied electronic level. The energy of the system is lowered because the electrons occupy the lower component. Furthermore, these relaxations are such that the vacancy exhibits negative electron correlation (negative-U). In particular, the V^+ charge state is unstable: the energy of the system is lowered when two V^+ convert to a V^0 and a V^{++} (Baraff *et al.*, 1979; Watkins and Troxell, 1980).

The self-interstitial can exist in several configurations, some of which are *simple*: the extra atom occupies one of the high-symmetry interstitial sites, such as the tetrahedral site, with small relaxations in the surrounding lattice. Other configurations are more complex and are known as *interstitialcies*: substantial lattice relaxations occur and the extra atom is not distinguishable. The lowest-energy configuration is an interstitialcy that consists of a dumbbell of atoms oriented in the $\langle 1\,1\,0 \rangle$ direction and occupying a nominal atomic site.

Both vacancies and self-interstitials contribute to self-diffusion. Vacancies migrate by simple jumps of the atoms nearest to the vacant site. The dynamical calculations of Car *et al.* (1992) found that at high temperatures there are also direct jumps of second-nearest and third-nearest neighbors across the six-member rings of the diamond lattice. Self-interstitials, in principle, migrate via a variety of paths, some of which are simple, such as the path through the tetrahedral and hexagonal interstitial sites, and some are interstitialcy paths that involve exchange of atoms (Car *et al.*, 1984). The most likely configuration of the interstitial, however, is the interstitialcy with lowest energy, which migrates via complex motions of the participating atoms (Blöchl *et al.*, 1993; Maroudas and Brown, 1993b).

The question of the relative contributions of vacancies and self-interstitials to self-diffusion has been debated intensely over the last 25 years. Experiments have only measured the self-diffusion coefficient, D_s, which obeys an Arrhenius relation of the form

$$D_s = D_0 \exp\left(-\frac{Q}{k_B T} \right) \tag{1}$$

where k_B is Boltzmann's constant, T is absolute temperature, D_0 is a preexponential factor with a much higher value than that typical for metals, and Q is the activation energy with values in the range of 4–5 eV (Seeger and Chik, 1968). The diffusion coefficient can be written as a sum of at least three terms:

$$D_s = \frac{c_I}{c_s} D_I + \frac{c_V}{c_s} D_V + D_X \tag{2}$$

where (c_I, c_V) and (D_I, D_V) are the concentrations and the diffusion coefficients of vacancies (V) and self-interstitials (I), respectively, c_s is the atomic concentration in the silicon crystal, and D_X is the diffusion coefficient for the concerted exchange mechanism which does not involve point defects (Pandey, 1986).

Atomic-scale calculations have provided information about these three contributions by direct computation of the equilibrium concentrations and the diffusion coefficients in eq. (2). The concentration of

an intrinsic point defect, either I or V, is written as

$$c_i(T) = c_s \exp\left(-\frac{G_i^f}{k_B T}\right), \quad i = \text{I, V} \tag{3}$$

where $G_i^f \equiv H_i^f - TS_i^f$, where H_i^f is the formation enthalpy, i.e. the enthalpy required to create a native lattice defect, and S_i^f is the formation entropy related to the phase-space volume accessible to the defect. According to transition-rate theory (Vineyard, 1957), the diffusion coefficent of an intrinsic point defect is written as

$$D_i(T) = \tfrac{1}{6} d_0^2 \tilde{\nu}_i \exp\left(-\frac{H_i^m}{k_B T}\right) \tag{4}$$

where d_0 is the bond length, $\tilde{\nu}_i$ is an effective attempt frequency, and H_i^m is the migration enthalpy of the defect equal to the difference between the formation enthalpies at the equilibrium and the saddle-point configurations, respectively (Girifalco, 1973).

Clearly, the key quantities are the formation enthalpies and entropies, which together determine the defect concentrations, and the migration enthalpies, which determine the defect diffusivities. The most detailed first-principles calculations by Blöchl *et al.* (1993) found that the formation energy of the self-interstitial is 3.3 eV, whereas that of the vacancy is 4.1 eV. Both defects have high formation entropies, in the range of $5–6k_B$. As a result, the interstitial concentration is much higher than that of the vacancy. The diffusivities of vacancies and interstitials are comparable at high temperatures, where they have been calculated (Blöchl *et al.*, 1993). Thus, the interstitial dominates self-diffusion largely because of its higher concentration. The contribution from the exchange mechanism is comparable to that of the vacancy.

In the computation of point defect diffusivities and equilibrium concentrations at finite temperatures, it has been proved practical to use a form of the harmonic approximation (Blöchl *et al.*, 1993; Maroudas and Brown, 1993a, b). These approximations, known as the local harmonic approximation (LHA) (LeSar *et al.*, 1989) and the quasi-harmonic approximation (QHA) (Lutsko *et al.*, 1988), are based on the approximate theory of the harmonic crystal (Ashcroft and Mermin, 1976), but incorporate fully anharmonic calculations of the total energy. The validity of these harmonic approximations was tested for the particular cases at hand. Blöchl *et al.* (1993) computed the anharmonic corrections to their LHA calculation of the free energy of vacancy formation and found them to be negligible at 500 K and to contribute 0.2 eV to the free energy at 1000 K. Maroudas and Brown (1993a) compared the result of the QHA for the perfect crystal with the exact free energy calculations of Broughton and Li (1987) and found that the approximation is valid up to temperatures $T \leqslant 0.75 T_m$, where $T_m = 1683$ K is the melting temperature of silicon.

As a further test of the quasi-harmonic approximation, we computed the temperature dependence of the specific heat at constant volume, $c_v(T)$. In the classical theory of the harmonic crystal, $c_v \equiv N^{-1}(\partial E/\partial T)_V$ is independent of temperature and equal to $3k_B$; this is the well-known law of Dulong and Petit (Ashcroft and Mermin, 1976). We computed $c_v(T)$ using the fully anharmonic results for the temperature dependence of the energy from the Monte Carlo simulations of Maroudas and Brown (1993a) with supercells that contain one vacancy or one interstitial, respectively. We found that $c_v = 3k_B$ is satisfied over the temperature range $50\text{ K} \leqslant T \leqslant 550\text{ K}$ to within an accuracy of 0.5%. Over the temperature range $600\text{ K} \leqslant T \leqslant 1200\text{ K}$, the computed specific heat increases above the harmonic value. The deviation from the harmonic result increases with temperature, but it does not exceed 5% at the highest temperature ($1200\text{ K} \simeq 0.71 T_m$) used in the comparison.

NORMAL-MODE ANALYSIS OF THE SELF-INTERSTITIAL MIGRATION

Calculations of transport properties of intrinsic point defects and their contribution to self-diffusion and impurity diffusion provide the necessary database for systematic analysis of mass transport in semiconductor crystals. The dynamical calculations also contain the details of all the atomic motions during the diffusive atomic jumps. Alternatively, one may wish to gain insights into the jump process by analyzing the motion in terms of the phonons of the crystal containing a point defect in its equilibrium configuration. In the process of jumping, the atom meets strong repulsive forces from its neighbors, so that it must surmount an energy barrier. The migrating atom acquires enough energy to climb this barrier as a result of a local thermal fluctuation consisting of a coming together of phonons of sufficient energy and appropriate directionality to move the atom over the barrier (Girifalco, 1973). In other words, an atomic jump can be viewed as a collective excitation of a select set of the normal modes of the atomic system.

In order to carry out such an analysis, the TH migration path was chosen because of its simplicity. This path involves the tetrahedral (T) and the hexagonal (H) sites. The interstitial atom located at the T and H sites is fourfold- and sixfold-coordinated, respectively. During the TH jump, the interstitial moves in a $\langle 1\,1\,1\rangle$ direction from a tetrahedral site to a nearest-neighbor tetrahedral site through the hexagonal site located at the midpoint between the two tetrahedral sites. This interstitial motion is shown in Fig. 1, with the unrelaxed silicon atoms on the $(0\,1\,\bar{1})$ plane of the diamond-cubic lattice. The TH migration path is characterized as simple (Car *et al.*, 1984) because it involves interstitial sites only, which is a characteristic of *channel diffusion*. Both simple and interstitialcy paths have been investigated in the literature (Car *et al.*, 1984; Bar-Yam and Joannopoulos, 1984a, b, c; Maroudas and Brown, 1993b).

The TH migration path of the self-interstitial in silicon has been investigated both by *ab initio* total energy calculations (Bar-Yam and Joannopoulos,

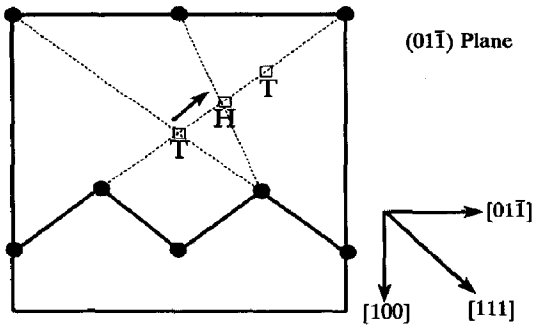

Fig. 1. The tetrahedral and hexagonal interstitial sites in a silicon lattice on a {1 1 0} plane. The dark dots indicate atoms in that plane. The arrow indicates the TH migration path.

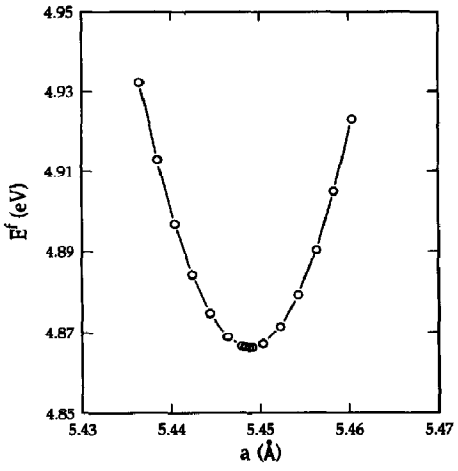

Fig. 2. Dependence of the formation energy of the self-interstitial at the tetrahedral site on the lattice parameter of the supercell used in the simulation.

1984a, b; Car *et al.*, 1984) and by atomistic simulations using interatomic potentials (Maroudas and Brown, 1993b). Maroudas and Brown (1993b) computed the Gibbs free energy of migration and the temperature dependence of the diffusion coefficient that corresponds to this path. In this work, the emphasis is on the normal modes of the equilibrium configuration, with the interstitial located at the tetrahedral site, and their contribution to atomic migration.

Equilibrium configuration and normal modes

The computational advantage of our calculation is that it solely relies on lattice statics and lattice dynamics simulations performed at $T = 0$ K. The calculation utilizes a cubic supercell of $N = 216 + 1$ atoms. The equilibrium configuration is computed starting from the perfect diamond lattice at $p = 0$, with a lattice parameter $a = 5.4309$ Å. The interstitial atom is put at the tetrahedral site closest to the center of mass of the supercell. Structural relaxation is performed by energy minimization with respect to the atomic coordinates using the steepest descent method (Gill *et al.*, 1981), while the atom at the geometrical origin of the supercell is kept fixed to avoid crystal translation.

After structural relaxation, volume relaxation is carried out by simple coordinate rescaling at different volumes to fix the lattice parameter to the value that corresponds to the minimum energy. The result of volume relaxation is shown in Fig. 2, where the formation energy of the interstitial is plotted as a function of the lattice parameter of the crystal; here, the lattice parameter a is defined in the same way as in the perfect diamond structure with eight atoms per conventional cubic unit cell, i.e. $a = (8/\rho)^{1/3}$, where ρ is the density of the crystal. The minimum energy occurs at a lattice parameter $a = 5.4487$ Å compared with $a = 5.4309$ Å for the perfect crystal. In all the following calculations, the volume of the supercell is kept fixed at the value that corresponds to this lattice parameter. The minimum energy corresponds to a formation energy of 4.87 eV for the tetrahedral interstitial, which is in excellent agreement with the value reported by Maroudas and Brown (1993a, b) who used a much more elaborate minimization scheme.

The lattice dynamics calculations are performed within the quasi-harmonic approximation. Let the $3N$-dimensional vectors $\mathbf{r}$ and $\mathbf{r}_0$ denote the atomic coordinates at some configuration and at the equilibrium configuration, respectively. The displacement vector $\mathbf{u}$ is defined as

$$\mathbf{u}(\mathbf{r}) \equiv \mathbf{r} - \mathbf{r}_0 . \tag{5}$$

In the harmonic approximation, which is asymptotically valid in the limit of small atomic displacements (Ashcroft and Mermin, 1976), the classical Hamiltonian is written as

$$\mathscr{H} = \Phi(\mathbf{r}_0) + \tfrac{1}{2}\mathbf{D}(\mathbf{r}_0):\mathbf{u}\mathbf{u} \tag{6}$$

where Φ is the potential energy and $\mathbf{D}(\mathbf{r}_0)$ is the Hessian of the interatomic potential evaluated at the equilibrium configuration, with elements

$$D_{ij,\alpha\beta} = \left(\frac{\partial^2 \Phi}{\partial r_{i,\alpha}\, \partial r_{j,\beta}}\right)_{\mathbf{r}_0} \tag{7}$$

where i and j refer to the ith and jth atoms and α and β are Cartesian indices. Writing Newton's equations of motion from eq. (6) and taking the Fourier transform in time gives

$$\mathbf{D}(\mathbf{r}_0)\cdot\mathbf{u}(\mathbf{r}) = m\omega^2\,\mathbf{u}(\mathbf{r}) \tag{8}$$

where $m = 4.6459 \times 10^{-26}$ kg is the mass of the common stable isotope ^{28}Si and ω is the angular frequency. Equation (8) describes an algebraic eigenvalue problem, the solution of which is the heart of the normal-mode analysis. We will refer to $\mathbf{D}(\mathbf{r}_0)$ as the dynamical matrix, because of its direct relation to the actual dynamical matrix at $\mathbf{k} = \mathbf{0}$; the dynamical matrix is defined in reciprocal space as the Fourier transform of $\mathbf{D}(\mathbf{r}_0)$ (Ashcroft and Mermin, 1976).

The symmetric dynamical matrix **D** was constructed for our system and its eigenvalues $\{\lambda_i, i = 1, \ldots, 3N\}$ and corresponding orthonormal eigenvectors $\{\mathbf{z}_i, i = 1, \ldots, 3N\}$ were computed by diagonalization (Wilkinson, 1965; Smith, 1974). The eigenvalues are related to the frequencies $\{\nu_i, i = 1, \ldots, 3N\}$ of the normal modes by

$$\nu_i = \frac{1}{2\pi}\sqrt{\frac{\lambda_i}{m}}. \tag{9}$$

The histogram of the phonon density of states $g(\omega)$ was calculated from the computed eigenfrequencies. Integrating the phonon density of states over the computed spectrum of angular frequencies gives the total number of normal modes as

$$\int_0^{\omega_{\max}} g(\omega)\,d\omega = 3N. \tag{10}$$

The histogram was computed both for the perfect crystal and the equilibrium configuration with the interstitial at the tetrahedral site. The results are shown in Fig. 3. Both histograms contain the three zero-frequency modes associated with pure translation of the crystal.

We observe that the presence of the self-interstitial causes a number of modifications to the phonon density of states of the perfect crystal. Whereas the positions of the main acoustic and optical phonon peaks remain largely unchanged, the region between them has a flatter density of states. In addition, acoustic states are pulled down in frequency, giving a higher density in the region of 2–5 THz, whereas optical states are pushed up in frequency, giving rise to a localized state above the perfect-crystal continuum.

Energetics of the TH interstitial jump

The energy variation along the adiabatic migration path is computed by structural relaxation after moving the interstitial along the [1 1 1] direction and fixing the appropriate degree of freedom at several locations along the path. Only one extra degree of freedom needs to be frozen for the calculation, namely the degree of freedom that specifies the [1 1 1] direction of the jump. Therefore, the jumping atom is allowed to relax on a plane perpendicular to the jump direction. This relaxation scheme is fully consistent with transition-rate theory (Girifalco, 1973; Lannoo and Bourgoin, 1982). The Cartesian coordinates of the atomic positions are mapped to a coordinate set with orthonormal basis the unit vectors along the [1 1 1], [1 $\bar{1}$ 0], and [$\bar{1}$ $\bar{1}$ 2] crystallographic axes. Keeping the [1 1 1]-coordinate of the interstitial fixed is the constraint for the energy minimization.

The results of the calculation are presented in Fig. 4, where the energy is plotted vs the distance from the original tetrahedral site. The hexagonal site is the position of the interstitial that corresponds to the saddle-point configuration. Defining the migration path coordinate η as

$$\mathbf{r}_I = \mathbf{r}_1 + \eta(\mathbf{r}_2 - \mathbf{r}_1), \quad 0 \leqslant \eta \leqslant 1 \tag{11}$$

where $\mathbf{r}_I$ is the position vector of the jumping interstitial and $\mathbf{r}_1$ and $\mathbf{r}_2$ are the position vectors of the initial and final equilibrium positions, respectively, gives the saddle-point configuration at $\eta = 0.50$. The

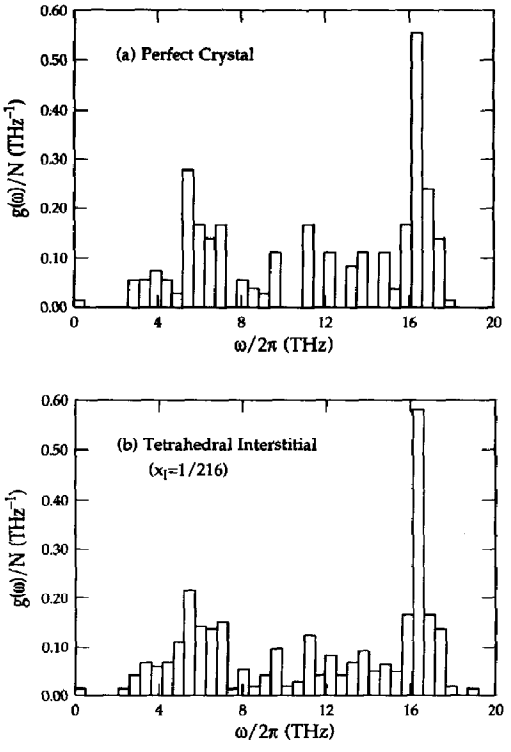

Fig. 3. Histogram of phonon density of states per atom for (a) the perfect crystal and (b) the tetrahedral interstitial configuration.

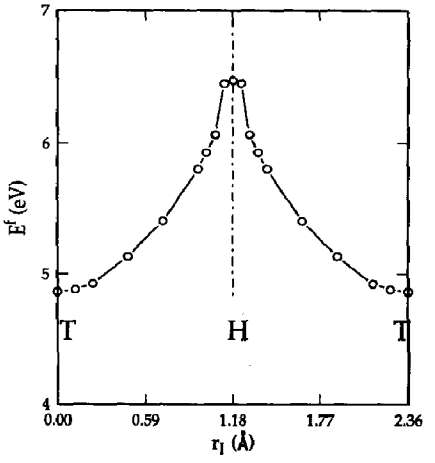

Fig. 4. Dependence of the energy of the interstitial on the distance along the TH migration path. The origin is the equilibrium position at a tetrahedral site.

computed formation energy of the hexagonal interstitial is 6.48 eV, resulting in an energy barrier for migration equal to 1.61 eV. The value for the formation energy of the hexagonal interstitial is lower by about 0.1 eV compared to previously reported energies using the SW interatomic potential (Batra *et al.*, 1987; Maroudas and Brown, 1993a, b) as a result of the efficient full structural relaxation of the saddle-point configuration performed in the present study.

Normal-mode analysis of the TH interstitial jump

The natural question that arises after the calculation of the normal modes of the crystal at the equilibrium configuration and the energy variation along the migration path is the possibility of existence of normal modes that dominate during the atomic jump. Therefore, the displacement vector $\mathbf{u}(\mathbf{r})$, eq. (5), is calculated for several atomic positions $\mathbf{r}$ along the migration path. The normal-mode analysis of the migration process consists of resolving the displacement vector $\mathbf{u}$ in the eigenvectors that correspond to the normal modes of the crystal at the equilibrium configuration as

$$\mathbf{u} = \sum_{i=1}^{3N} c_i \mathbf{z}_i . \tag{12}$$

Constructing the linear combination (12) is always possible because the eigenvectors $\{\mathbf{z}_i\}$ form a linearly independent complete set. For the calculation of the coefficients $\{c_i, i = 1, \ldots, 3N\}$ in the linear combination, eq. (12) is written as

$$\mathbf{Z} \cdot \mathbf{c} = \mathbf{u} \tag{13}$$

where $\mathbf{c}$ is the $3N$-dimensional vector of the coefficients $\{c_i\}$ and $\mathbf{Z}$ is the matrix of the eigenvectors, i.e. a matrix of order $3N$ containing the orthonormal eigenvectors of the dynamical matrix $\mathbf{D}(\mathbf{r}_0)$; the eigenvector in column i of matrix $\mathbf{Z}$ corresponds to the eigenfrequency ν_i. Before solving eq. (13), the order of the problem is reduced to $3N - 3 = 648$ by eliminating the first three columns of $\mathbf{Z}$ that correspond to the zero-frequency purely translational modes and the first three rows that give the zero displacements of the fixed particle in the geometrical origin of the supercell.

Equation (13) is solved by direct LU factorization (Dahlquist and Björck, 1974) and normal modes with significant contributions to the displacement $\mathbf{u}$ were identified using the criterion $|c_i| > 10^{-2}$. The dominant mode is defined as

$$|c_i| \equiv \max_j \{|c_j|\}, \quad j = 4, \ldots, 3N . \tag{14}$$

The results of the normal-mode analysis are presented in Table 1, where the number of significant modes and the frequency of the dominant mode are given for the values of η that were investigated. Two interesting conclusions are drawn from the results of Table 1. First, there is a pronounced *mixing* of normal modes as the interstitial displacement from the equilibrium position increases, i.e. as η increases. Therefore, the number of significant modes increases from 4 (out of 648) at $\eta = 0.05$ to 63 at the saddle-point configuration. Second, the dominant mode in all cases is one of the modes that correspond to the threefold-degenerate lowest nonzero eigenfrequency ν_1. Therefore, there is a single normal mode that dominates throughout the migration path. This corresponds to a number n of phonons with the appropriate energy $(n + 1/2)h\nu_1$, where h is Planck's constant, and directionality that helps the jumping interstitial overcome the energy barrier of 1.61 eV.

Table 1. Number of normal modes with significant contributions to the atomic displacements and frequency that corresponds to the dominant mode as a function of the TH migration path coordinate

η	Number of significant modes	Frequency of dominant mode (Hz)
0.05	4	$\nu_1 = 2.16 \times 10^{12}$
0.10	14	$\nu_1 = 2.16 \times 10^{12}$
0.20	26	$\nu_1 = 2.16 \times 10^{12}$
0.30	37	$\nu_1 = 2.16 \times 10^{12}$
0.40	41	$\nu_1 = 2.16 \times 10^{12}$
0.50	63	$\nu_1 = 2.16 \times 10^{12}$

For values of η up to 0.40 the most significant modes correspond to the threefold-degenerate eigenfrequencies $\nu_1 = 2.16$, $\nu_2 = 2.90$, $\nu_5 = 3.16$, and $\nu_{10} = 3.38$ THz. Here, the subscripts are used in ascending order above the threefold-degenerate zero eigenfrequency that corresponds to pure crystal translation. All these frequencies correspond to phonons of the acoustic branches of the crystal with a dispersion relation that goes asymptotically to $\omega = Ck$ as $k \to 0$, which is the dispersion relation characteristic of sound waves at small wavenumbers k with C being the speed of sound in the solid. In addition, these four frequencies correspond to normal modes with the appropriate directionality in displacing the interstitial atom along the [1 1 1] direction of the migration path. In particular, in all four cases the linearly independent eigenvectors that correspond to the threefold-degenerate eigenfrequencies give interstitial displacements along the $[\bar{1}\,1\,0]$, $[\bar{1}\,\bar{1}\,2]$, and [1 1 1] directions. Obviously, the dominant contributions to $\mathbf{u}(\eta)$ come only from the normal modes that displace the interstitial in the [1 1 1] direction.

To quantify the contribution of the normal modes that correspond to the four dominant eigenfrequencies, we define weighting factors w_i, $i = 1, 2, 5, 10$, as

$$w_i \equiv \frac{1}{\|\mathbf{c}\|_2^2} \left(\sum_{j=3i-2}^{3i} c_j^2 \right) \tag{15a}$$

where $\|\mathbf{c}\|_2$ is the Euclidean norm of the solution vector $\mathbf{c}$, eq. (13), defined as

$$\|\mathbf{c}\|_2 \equiv \left(\sum_{i=1}^{3N-3} c_i^2 \right)^{1/2} \tag{15b}$$

Figure 5 shows the variation of these weighting factors with the migration path coordinate η. The varia-

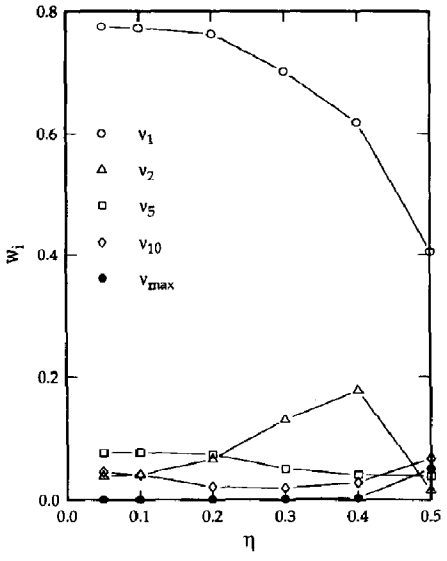

Fig. 5. Weighting factors for the normal modes that contribute significantly to the atomic displacements along the TH migration path. The abscissa is the migration path coordinate η.

tion of the weighting factor w_{max} corresponding to the threefold-degenerate maximum eigenfrequency ν_{max} is also plotted in Fig. 5. The three eigenvectors that correspond to ν_{max} give interstitial displacements along the $[\bar{4}\,\bar{1}\,5]$, $[2\,\bar{3}\,1]$, and $[1\,1\,1]$ crystallographic directions with the dominant contributions from the normal mode that displaces the interstitial in the $[1\,1\,1]$ direction of the jump. We added this frequency in the analysis because of its identification as eigenfrequency of high-energy localized modes in Fig. 3(b). Indeed, the weighting factor w_{max} becomes significant when the saddle-point configuration is approached, although it is negligible at low η. Figure 5 shows that the weighting factor w_1 is the highest for all values of η with a contribution of about 80% for $\eta < 0.10$ and falling to a contribution of 40% at the saddle point. The variation of the weighting factors w_2, w_5, and w_{10} with η shows the extent of mixing of phonon modes as the displacement from the equilibrium configuration increases. The values of w_5 and w_{10} never exceed 10% and only the value of w_2 that corresponds to the second lowest eigenfrequency reaches levels of 10–20% at intermediate values of η.

To conclude the normal-mode analysis of interstitial migration along the TH path, the variation of the crystal energy with interstitial displacement from its equilibrium position is computed by exciting the crystal above the energy level of the equilibrium configuration according to atomic displacements that correspond to dominant normal modes. All the atoms in the supercell are displaced from their equilibrium positions proportionally to the displacements that correspond to the dominant normal modes. It should be underlined here that the actual anharmonic energies are computed (according to the SW interatomic potential) and not only the quadratic term that appears in the harmonic Hamiltonian of eq. (6). The results of this analysis are presented in Fig. 6, together with the actual energy variation along the TH path. The energy curve that corresponds to the dominant mode of frequency ν_1 remains tangent to the actual energy curve of the migration path up to $\eta = 0.08$, i.e. an interstitial displacement of 0.19 Å from the equilibrium position. The energy curves that correspond to the modes of frequencies ν_2, ν_5, ν_{10}, and ν_{max} deviate from the actual energy curve almost immediately. However, in spite of the clear dominance of the normal mode corresponding to ν_1 it would be impossible to construct the actual energy curve solely by this mode.

An important component in the application of transition-rate theory in the calculation of diffusion coefficients is the calculation of the effective jump frequency $\tilde{\nu}$ introduced in eq. (4). In the harmonic approximation, $\tilde{\nu}$ is defined as

$$\tilde{\nu} \equiv \frac{\prod_j \nu_j}{\prod_j \nu_j^*} \tag{16}$$

where ν_j and ν_j^* are the normal-mode frequencies at the equilibrium and the saddle-point configuration, respectively. There is one degree of freedom missing from the product in the denominator of eq. (16), which corresponds to the fixed coordinate of the jumping atom in the direction of the jump. We computed $\tilde{\nu}$ for the TH jump of the interstitial by diagonalizing the dynamical matrix at the saddle-point configuration also. We found a value of $\tilde{\nu} = 1.31 \times 10^{13}$ Hz. This value of the effective attempt frequency corresponds to the lowest frequency of the optical branch, i.e. the frequency value at point X in k-space (Broughton and Li, 1987).

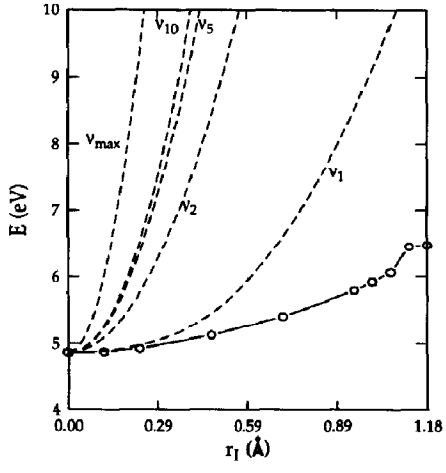

Fig. 6. Variation of crystal energy with interstitial displacement from its equilibrium position by excitation according to the normal modes of frequencies ν_1, ν_2, ν_5, ν_{10}, and ν_{max}. The actual energy variation along the TH path is also shown.

CRYSTALLINE SILICON WITH HIGH CONTENT OF POINT DEFECTS VS AMORPHOUS SILICON

Fundamental understanding of the structure and properties of amorphous materials is a real challenge to most of the conventional theoretical techniques of solid state physics due to the lack of periodicity compared to crystalline solids. Amorphous semiconductors are not completely disordered on the atomic scale. They exhibit almost rigorous bond-length and bond-angle constraints on the nearest-neighbor environment. Amorphous semiconductors do not consist of close-packed atoms, but contain covalently bonded atoms arranged in an open network with correlations in ordering up to the third- or fourth-nearest neighbors; this short-range order is directly responsible for observable semiconductor properties (Brodsky, 1979).

Amorphous silicon (a-Si) has been extensively studied both experimentally (Tan *et al.*, 1972; Brodsky *et al.*, 1972; Brodsky, 1979; Fortner and Lannin, 1988) and theoretically (Wooten *et al.*, 1985; Pantelides, 1986, 1987; Broughton and Li, 1987; Car and Parrinello, 1988; Buda *et al.*, 1989; Kwon *et al.*, 1991) for the fundamental interest that presents as a prototypical covalently bonded amorphous semiconductor and as the most promising material for a wide range of applications of solar energy conversion. In practice, amorphous semiconductors are prepared in the form of thin films by atomic deposition procedures (Brodsky, 1979) or even by irradiation (Bhadra *et al.*, 1988). In theory, the computer generation of a realistic amorphous structure is an equally challenging process by either *ab initio* methods or interatomic potentials in conjunction with molecular dynamics (Ding and Andersen, 1986; Car and Parrinello, 1988) or Monte Carlo techniques (Wooten *et al.*, 1985) that allow simulation of thermal treatments similar to laboratory preparations.

The theoretical interest on the role of self-interstitials in the amorphization process of silicon is recent (Torres *et al.*, 1987; Schober, 1989; Maroudas and Brown, 1993a). This interest was motivated by similarities between amorphous materials with interstitials in metals, which exhibit properties as those expected for glassy materials, such as two-level systems and quasi-localized vibrations at low frequencies (Erhart *et al.*, 1986), as well as by recent findings on the role of self-interstitials in the amorphization of alloys (Sabochick and Lam, 1990). Torres *et al.* (1987) proposed a model for a particular extended interstitial structure in crystalline silicon (c-Si) with ring structure characteristic of a-Si and low-energy excitations for reasons of symmetry and suggested that this defect may act as a nucleus for amorphization under irradiation. In addition, Schober (1989) reported a detailed structural study of extended interstitials in silicon and germanium using several interatomic potentials leading to similar conclusions for the role of interstitials in the amorphization process. More recently, Maroudas and Brown (1993a) pointed out similarities in the temperature dependence of the density of crystalline systems heavily supersaturated with point defects with the amorphous phase.

Motivated by the above theoretical results, we present a comprehensive study of the similarities between a-Si and c-silicon with high densities of self-interstitials. In the periodic supercell approach that is adopted here, increasing the interstitial concentration corresponds to the use of a smaller supercell for the calculation. We have used two cubic supercells with $N = 216 + 1$ and $N = 64 + 1$ atoms. The properties used for comparison with the amorphous phase are the density, the nearest-neighbor coordination and bond lengths, and vibrational properties including the phonon density of states.

Model of amorphous silicon used for comparison

As was done by Maroudas and Brown (1993a), we used the model structure of a-Si constructed by Wooten *et al.* (1985) for our comparisons. We will refer to this structure as WWW a-Si. The WWW algorithm generates realistic random network models of a-Si with periodic boundary conditions. The algorithm starts from the diamond structure and repeatedly rearranges the local structure randomly by preserving tetrahedral bonding and introducing fivefold and sevenfold rings. The algorithm proceeds in making several topological relaxations of this type to reduce the energy and employs the simulated annealing method (Kirkpatrick *et al.*, 1983) for sufficient relaxation. Wooten *et al.* (1985) succeeded in reproducing the radial distribution function of amorphous germanium using the Keating potential (Keating, 1966). The results of Wooten *et al.* (1985) are also in good agreement with the *ab initio* molecular-dynamics simulations for a-Si of Car and Parrinello (1988), who used a detailed thermal treatment to produce the amorphous phase starting from the liquid.

Broughton and Li (1987) carried out molecular-dynamics simulations for WWW a-Si using the SW interatomic potential. They showed that the density of WWW a-Si is about 1% lower than the crystal density in agreement with experiment (Brodsky *et al.*, 1972); the lower density of the amorphous phase is a common feature of elemental semiconductors (Paul *et al.*, 1973). Also, the computed bond-angle distribution function (Broughton and Li, 1987) is in fairly good agreement with the *ab initio* molecular-dynamics simulations of Buda *et al.* (1989), who generated a-Si by using an even slower rate of quenching from the melt than the rate used by Car and Parrinello (1988). The WWW a-Si undergoes a phase transition at $p = 0$ either to the liquid or to the crystal at temperatures above 1000 K (Broughton and Li, 1987). In spite of the failure of the SW interatomic potential to describe the amorphous-to-liquid phase transition (Broughton and Li, 1987), the above properties of WWW a-Si constitute a reasonable representation of the amorphous phase for comparison with our interstitial calculations.

Temperature dependence of the density

The temperature dependence at $p = 0$ of the density of silicon crystals supersaturated with vacancies or self-interstitials was computed by Monte Carlo simu-

lations by Maroudas and Brown (1993a). We include these results here for completeness. It should also be noted that the self-interstitials correspond to the lowest-energy extended interstitial configuration. Figure 7 shows the temperature dependence of the density for two crystals with vacancy atomic fractions $x_V = 1/216$ and $1/64$, respectively, and two crystals with interstitial atomic fractions $x_I = 1/216$ and $1/64$, respectively. These are very high concentrations of point defects when compared to the equilibrium concentrations, which do not exceed an atomic fraction of 10^{-7} at temperatures close to the melting point (Blöchl *et al.*, 1993; Maroudas and Brown, 1993a). Decreasing the vacancy or the interstitial concentration in the calculation by increasing the size of the supercell makes the corresponding curves approach the curve for c-Si. The interesting conclusion is that increasing the interstitial concentration at constant pressure decreases the crystal density toward the density of the amorphous structure.

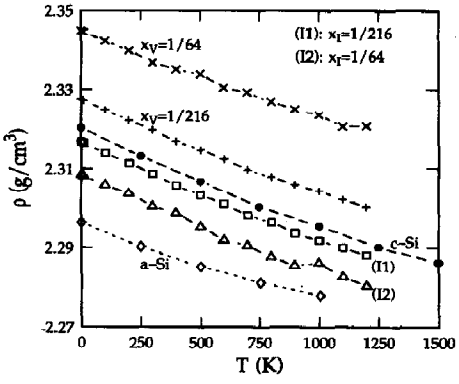

Fig. 7. Dependence on temperature of the densities of crystalline and amorphous silicon (WWW a-Si) and silicon crystals supersaturated with vacancies and self-interstitials at different concentrations from Maroudas and Brown (1993a). The results for WWW a-Si are taken from Broughton and Li (1987).

Table 2. Values of ρ/ρ_c for crystals containing different atomic fractions of point defects and for a-Si

Structure	ρ/ρ_c
$x_V = 1/64$	1.0106
$x_V = 1/216$	1.0032
$x_I = 1/216$	0.99845
$x_I = 1/64$	0.99493
WWW a-Si	0.98966
a-Si (exp.)	0.99
a-Ge (exp. $T = 623$ K)	0.97

Note: ρ_c is the value of the density of crystalline silicon and is used to scale the densities ρ of the other structures. The density for WWW a-Si is taken from Broughton and Li (1987). The experimental values for amorphous silicon and amorphous germanium are taken from Brodsky *et al.* (1972) and Paul *et al.* (1973).

This tendency in the density of the crystal to approach the density of the amorphous phase is further demonstrated by comparing the ratio of the densities over the perfect crystal density, ρ_c. The comparison carried out at $T = 0$ K is shown in Table 2; all the $\rho(T)$ curves in Fig. 7 run almost in parallel. A final conclusion from this comparison is that increasing the vacancy concentration leads to further increase of the density compared to the perfect crystal, which is already higher than the density of a-Si by 1%. Therefore, the investigation of the properties of silicon crystals heavily supersaturated with vacancies is not pursued any further.

Nearest-neighbor coordination

One useful way in which to compare the amorphous phase with a crystal that is heavily supersaturated with interstitials is by computing the percentage of atoms with given nearest-neighbor coordination. Unfortunately, one cannot determine unambiguously which atoms are nearest neighbors, second-nearest neighbors, etc. Figure 8 shows the radial distribution functions, $g(r)$, for the two crystals with $x_I = 1/216$ and $x_I = 1/64$. Contrary to the radial distribution function of the liquid or the superheated crystal (Stillinger and Weber, 1985) the radial distribution functions of Fig. 8 do not exhibit a *strong* minimum between the first two main peaks. The small fluctuations that are evident between the first two sharp peaks suggest that one cannot differentiate nearest

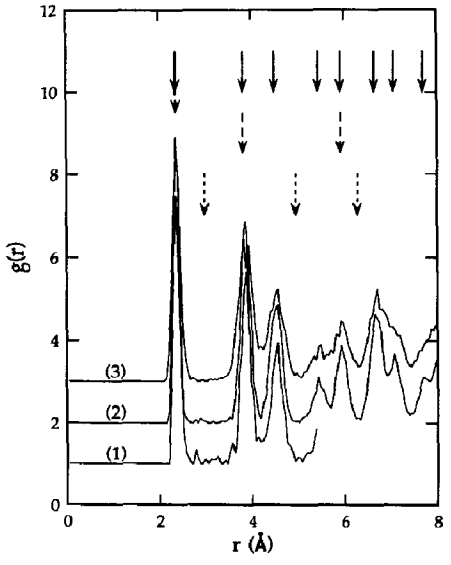

Fig. 8. Radial distribution functions of crystals with interstitial concentrations (1) $x_I = 1/64$ at $T = 500$ K, (2) $x_I = 1/216$ at $T = 500$ K, and (3) $x_I = 1/216$ at $T = 1000$ K. The radial resolution in the calculation is 0.05 Å. Solid and dashed arrows indicate peak positions in the radial distribution function of the perfect crystalline structure and of the WWW a-Si structure, respectively. Dotted arrows indicate minima in the radial distribution function of WWW a-Si. The results for WWW a-Si are taken from Broughton and Li (1987).

from next-nearest neighbors by taking the first minimum after the first peak as demarcation. Therefore, we adopted the alternative approach of using as demarcation the average of the radii that correspond to the first two main peaks of $g(r)$. This radius, $r_m = 3.12$ Å, is very close to the radius, $r = 2.99$ Å, that corresponds to the first minimum in the radial distribution function of the WWW a-Si at $T = 750$ K (Broughton and Li, 1987); we found the variation of r_m with temperature to be negligible over the range $500\ \text{K} \leqslant T \leqslant 1200$ K. In general, the positions of the peaks and valleys in the radial distribution functions of the two crystals remain largely unchanged over the same temperature range.

Figure 9 shows the histogram for the bond-length distribution of the two crystals with $x_I = 1/216$ and 1/64, respectively. Most of the bonds have lengths close to the bond length of 2.36 Å of the perfect crystalline structure. The significant fraction of bonds with lengths between 2.26 and 2.30 Å and between 2.40 and 2.80 Å is a result of the atomic rearrangement around the extended interstitial, which is not a simple local rearrangement. The presence of weak bonds with lengths between 2.80 and 3.12 Å is very rare. This latter result is comparable with the result reported by Car and Parrinello (1988), who used a 54-atom supercell in their *ab initio* molecular-dynamics simulation of a-Si. Car and Parrinello (1988) identified only two weak bonds with lengths varying from 2.7 to 3.1 Å and from 2.4 to 3.35 Å, respectively, during the course of the simulation. The position of the first minimum of the radial distribution function in their calculation was $r_m = 2.75$ Å (Car and Parrinello, 1988).

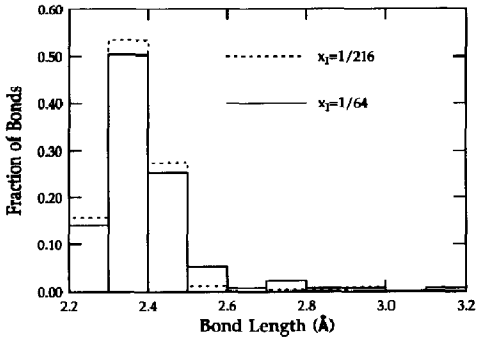

Fig. 9. Histogram for the bond-length distribution of crystals with interstitial concentrations $x_I = 1/216$ and 1/64, respectively.

The results for the percentage of atoms with given coordination are presented in Table 3. The values given in the last column of Table 3 were obtained by Broughton and Li from a molecular-dynamics simulation at 750 K. We calculated the values given in the other two columns and found them to be insensitive over the range $500\ \text{K} \leqslant T \leqslant 1200$ K. In both crystals, fourfold coordination clearly dominates, which is also the case for WWW a-Si (Broughton and Li, 1987). However, as the interstitial concentration increases, the fraction of fivefold-coordinated atoms increases and becomes comparable with the corresponding fraction in WWW a-Si. These results are consistent with the suggestion that fivefold-coordinated silicon atoms are a dominant intrinsic defect in a-Si (Pantelides, 1986).

Vibrational properties

The vibrational properties of the two crystals with high interstitial concentrations were calculated by diagonalizing the corresponding dynamical matrices at the equilibrium configurations. The equilibrium configurations were obtained by an elaborate relaxation procedure based on a combination of a variation of simulated annealing with quenching by the steepest descent method (Maroudas and Brown, 1993a). First, the sum of the logarithms of the normal-mode frequencies per atom are compared with the result for the WWW a-Si computed by Broughton and Li (1987). These results are presented in Table 4 and show the gradual decrease of the sum from the perfect crystalline to the amorphous phase through the crystal structures that are heavily supersaturated with interstitials. In the context of the harmonic approximation (Girifalco, 1973), this decrease implies the corresponding gradual increase in the vibrational entropy. The exact same trend in the cohesive energy from the perfect crystalline to the amorphous phase also is shown in Table 4; the term cohesive energy applies to the zero-temperature energy and is used here as an average energy per atom in the crystals with high interstitial concentrations.

Table 3. Percentage of atoms with given coordination for crystals with interstitial concentrations $x_I = 1/216$ and $x_I = 1/64$

Coordination	Percentage of atoms			
	c-Si	$x_I = 1/216$	$x_I = 1/64$	WWW a-Si
3	0	0.0	0.0	1.2
4	100	95.8	87.7	86.6
5	0	3.2	10.8	11.8
6	0	0.5	0.0	0.2
7	0	0.5	1.5	—

The results for WWW a-Si are taken from Broughton and Li (1987).

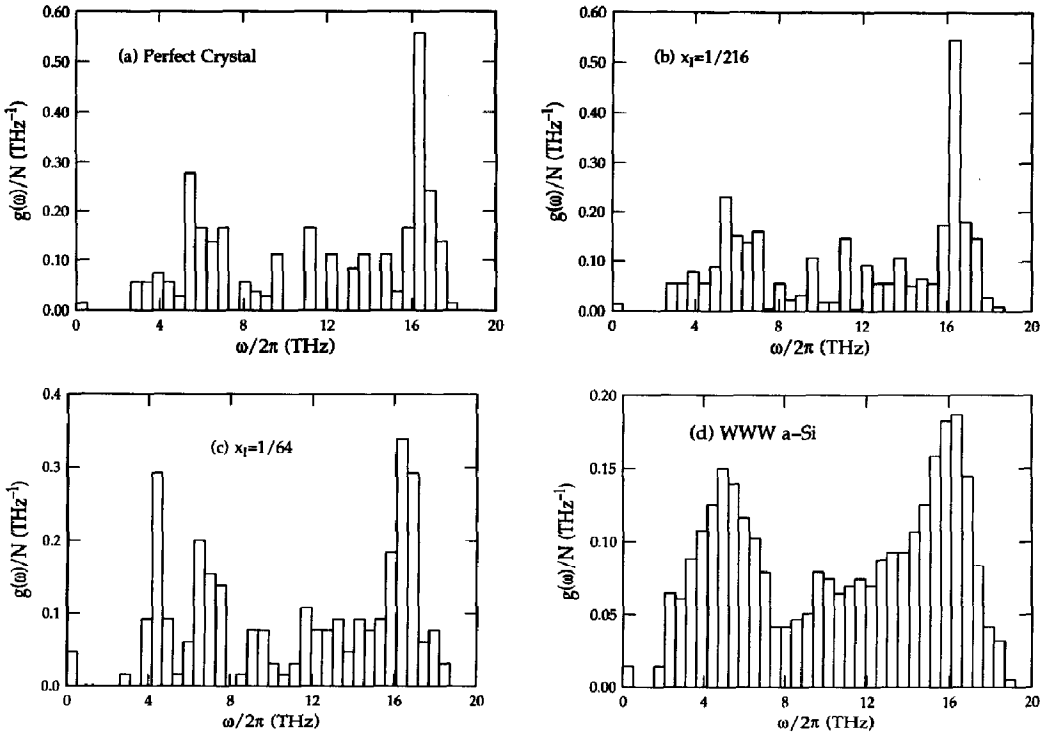

Fig. 10. Histograms of phonon density of states per atom for the (a) perfect crystal, (b) crystal with $x_I = 1/216$, (c) crystal with $x_I = 1/64$, and (d) WWW a-Si. The last histogram is reproduced from Broughton and Li (1987).

Table 4. Sum of the logarithms of the normal-mode frequencies per atom and cohesive energies for the perfect crystal, the two crystals with interstitial concentrations $x_I = 1/216$ and 1/64, respectively, and for WWW a-Si

Structure	$N^{-1}\Sigma \ln(\nu_i/\nu_0)$	Cohesive energy (eV/atom)
c-Si	4.7553	− 4.33
$x_I = 1/216$	4.7421	− 4.32
$x_I = 1/64$	4.7017	− 4.28
WWW a-Si	4.4546	− 4.12

The frequency ν_0-used for scaling purposes is characteristic of the SW interatomic potential used in the calculations.

The histograms of the phonon density of states for the two crystals with high interstitial concentrations are presented in Fig. 10 together with the corresponding histogram for the perfect crystal and for the WWW model of a-Si as computed by Broughton and Li (1987). The trends in the histograms are quite evident. There is a shift of acoustic states to lower frequencies and a shift of optical states to higher frequencies with a relative flattening of the density of states between the main peaks. This overall trend is consistent with the features of the phonon density of states of the WWW model of a-Si except for one significant difference. In the case of the crystal with $x_I = 1/64$, the acoustic peak is clearly split into two peaks, suggesting that there is considerably more disorder in a-Si than there is in a crystal with high interstitial concentrations. On the other hand, we note that the overall height of the density of the acoustic states gradually becomes comparable to that of the optical states, which is again consistent with what is calculated for the WWW model of a-Si.

SUMMARY AND CONCLUSIONS

The properties of the vacancy and the self-interstitial in silicon have been established by a combination of experimental and theoretical techniques. The vacancy has primarily intriguing electronic properties, especially its negative-U behavior which arises from charge-dependent lattice relaxations. On the other hand, the interstitial is the most interesting intrinsic point defect in silicon because of the multiplicity in its stable configurations and the possibility to follow many different paths during migration. Furthermore, the evidence so far strongly supports the conclusion that self-interstitials dominate self-diffusion.

In this paper, we carried out a detailed analysis of one of the migration paths of the self-interstitial and elucidated the participation of phonons in the atomic jump process. Although the analysis was exclusively focused on the TH path for interstitial migration, our methodology is quite robust and, therefore, applicable to interstitialcy paths and vacancy jumps. Our analysis showed that only a few normal modes that

correspond to phonons with the appropriate energy and directionality participate significantly in the migration process. Among these few modes, only the one that corresponds to the phonon of lowest energy is dominant throughout the migration path. However, the admixture of many phonon modes is essential to produce an adiabatic atomic migration.

Finally, we compared the properties of a model structure of amorphous silicon with those of a silicon crystal with increasingly higher concentrations of point defects. In the latter case, the level of intrinsic point defects was highly nonequilibrium. Extensive lattice relaxations are responsible for the counter-intuitive result that the density increases with increasing vacancy concentration, while it decreases toward the density of the amorphous phase with increasing interstitial concentration. Furthermore, increasing the interstitial concentration in the crystal decreases the percentage of atoms with fourfold coordination and increases the percentage of atoms with fivefold coordination approaching the corresponding percentages of the model amorphous phase. Moreover, the same tendency appears in the vibrational properties including vibrational entropies and the position and densities of the acoustic and optical peaks in the phonon-density-of-states histograms. Thus, there is a good reason to believe that amorphous silicon has many structural properties that resemble high concentrations of self-interstitials in crystalline silicon. These results, however, do not necessarily establish the dominant role of self-interstitials in the amorphization process.

In spite of the similarities between silicon crystals with very high concentrations of self-interstitials and amorphous silicon, the structural disorder in a-Si is considerably higher. In the supercell approach that was adopted here, a regular distribution of self-interstitials is generated, where increase in the interstitial concentration is equivalent to decreasing the supercell size. In such a representation, the disorder arises due to the pronounced relaxations around the interstitial, while the long-range order of the crystalline structure is retained. Furthermore, the use of increasingly smaller supercells puts the emphasis on the short-range rather than the long-range order. In such a case, however, the interstitials are not truly isolated point defects anymore. The resulting defect interactions is the main feature of a system with high defect concentration. The reported similarities in the structural, vibrational and thermodynamic properties of the amorphous structure with the crystals with a regularly distributed large interstitial population underlines the tendency of the crystalline structure toward the amorphous structure at a high concentration of self-interstitials. Considerably higher disorder in the long-range structure would be expected for a random distribution of a large number of self-interstitials within a large simulation cell.

Acknowledgements—This work was supported in part by the Office of Naval Research under Contract No. N00014-92-C-0085. All the computations were performed using the AGORA RS/6000 workstation network maintained by IBM Research Division. The authors acknowledge useful discussions with Dr D. B. Laks. One of the authors (D. M.) gratefully acknowledges the support of Professor Robert A. Brown of the Chemical Engineering Department at MIT during the course of his Ph.D. research, when calculations of several configurations used in the present study were performed.

NOTATION

a	lattice parameter, Å
c_I	concentration of self-interstitials, cm^{-3}
c_s	concentration of lattice sites, cm^{-3}
c_V	concentration of vacancies, cm^{-3}
c_v	specific heat at constant volume, $J K^{-1}$
C	speed of sound, $m s^{-1}$
d_0	bond length, Å
D_0	preexponential factor for self-diffusion coefficient, $m^2 s^{-1}$
D_I	diffusion coefficient of self-interstitials, $m^2 s^{-1}$
D_s	self-diffusion coefficient, $m^2 s^{-1}$
D_V	diffusion coefficient of vacancies, $m^2 s^{-1}$
D_X	diffusion coefficient for concerted exchange mechanism, $m^2 s^{-1}$
$\mathbf{D}$	dynamical matrix, $J m^{-2}$
E	energy, eV
$g(r)$	radial distribution function
$g(\omega)$	phonon density of states, $rad^{-1} s$
G_i^f	Gibbs free energy of formation of type-i defect, eV
h	Planck's constant, J s
H_i^f	formation enthalpy of type-i defect, eV
H_i^m	migration enthalpy of type-i defect, eV
$\mathscr{H}$	crystal Hamiltonian, J
k_B	Boltzmann's constant, $eV K^{-1}$
$\mathbf{k}$	wave vector, m^{-1}
m	atomic mass, kg
N	number of atoms in supercell
Q	activation energy for self-diffusion, eV
$\mathbf{r}$	vector of atomic coordinates, Å
$\mathbf{r}_0$	vector of atomic coordinates at the equilibrium configuration, Å
$\mathbf{r}_I$	position vector of migrating interstitial atom, Å
S_i^f	formation entropy of type-i defect, $eV K^{-1}$
T	temperature, K
$\mathbf{u}$	displacement vector, Å
U	electron–electron correlation energy, eV
V	volume, m^{-3}
w_i	weighting factor for the ith normal mode
x_I	atomic fraction of self-interstitials
x_V	atomic fraction of vacancies
$\mathbf{z}_i$	eigenvector of the ith normal mode, Å
$\mathbf{Z}$	matrix of eigenvectors of the normal modes, Å

Greek letters

η	migration path coordinate
λ_i	eigenvalue of the ith normal mode, $kg rad^2 s^{-2}$

$\tilde{\nu}$ effective attempt frequency, s^{-1}
ν_i frequency of the ith normal mode, s^{-1}
ν_i^* frequency of the ith normal mode at the saddle-point configuration, s^{-1}
ρ density, $g\,cm^{-3}$
ρ_c density of perfect crystal, $g\,cm^{-3}$
Φ potential energy, J
ω_i angular frequency of the ith normal mode, rad s^{-1}

REFERENCES

Ashcroft, N. W. and Mermin, N. D., 1976, *Solid State Physics*. Saunders College, Philadelphia.

Balluffi, R. W. and Granato, A. V., 1979, Dislocations, vacancies and interstitials, in *Dislocations in Solids* (Edited by F. R. N. Nabarro), Vol. 4, pp. 1–133. North-Holland, Amsterdam.

Baraff, G. A., Kane, E. O. and Schlüter, M., 1979, Silicon vacancy: a possible Anderson negative-*U* system. *Phys. Rev. Lett.* **43**, 956–959.

Bar-Yam, Y. and Joannopoulos, J. D., 1984a, Barrier to migration of the silicon self-interstitial. *Phys. Rev. Lett.* **52**, 1129–1132.

Bar-Yam, Y. and Joannopoulos, J. D., 1984b, Electronic structure and total energy migration barriers of silicon self-interstitials. *Phys. Rev.* **B30**, 1844–1854.

Bar-Yam, Y. and Joannopoulos, J. D., 1984c, Silicon self-interstitial migration: multiple paths and charge states. *Phys. Rev.* **B30**, 2216–2218.

Baskes, M. I., 1987, Application of the embedded-atom method to covalent materials: a semiempirical potential for silicon. *Phys. Rev. Lett.* **59**, 2666–2669.

Baskes, M. I., 1992, Modified embedded-atom potentials for cubic materials and impurities. *Phys. Rev.* **B46**, 2727–2742.

Batra, I. P., Abraham, F. F. and Ciraci, S., 1987, Molecular dynamics study of self-interstitials in silicon. *Phys. Rev.* **B35**, 9552–9558.

Bhadra, R., Pearson, J., Okamoto, P., Rehn, L. and Grimsditch, M., 1988, Elastic properties of Si during amorphization. *Phys. Rev.* **B38**, 12656–12659.

Biswas, R. and Hammann, D. R., 1985, Interatomic potentials for silicon structural energies. *Phys. Rev. Lett.* **55**, 2001–2004.

Blöchl, P. E., Smargiassi, E., Car, R., Laks, D. B., Andreoni, W. and Pantelides, S. T., 1993, First-principles calculations of self-diffusion constants in silicon. *Phys. Rev. Lett.* **70**, 2435–2438.

Brodsky, M. H. (Ed.), 1979, Introduction, *Amorphous Semiconductors*, pp. 1–7. Springer, Berlin.

Brodsky, M. H., Kaplan, D. and Ziegler, J. F., 1972, Densities of amorphous Si films by nuclear backscattering. *Appl. Phys. Lett.* **21**, 305–307.

Broughton, J. Q. and Li, X. P., 1987, Phase diagram of silicon by molecular dynamics. *Phys. Rev.* **B35**, 9120–9127.

Buda, F., Chiarotti, G. L., Stich, I., Car, R. and Parrinello, M., 1989, *Ab initio* molecular dynamics of liquid and amorphous semiconductors. *J. Non-Cryst. Solids* **114**, 7–12.

Car, R., Blöchl, P. and Smargiassi, E., 1992, *Ab initio* molecular dynamics of semiconductor defects. *Mater. Sci. Forum* **83–87**, 433–446.

Car, R., Kelly, P. J., Oshiyama, A. and Pantelides, S. T., 1984, Microscopic theory of atomic diffusion mechanisms in silicon. *Phys. Rev. Lett.* **52**, 1814–1817.

Car, R. and Parrinello, M., 1988, Structural, dynamical, and electronic properties of amorphous silicon: an *ab initio* molecular-dynamics study. *Phys. Rev. Lett.* **60**, 204–207.

Chelikowsky, J. R., Phillips, J. C., Kamal, M. and Strauss, M., 1989, Surface and thermodynamic interatomic force fields for silicon clusters and bulk phases. *Phys. Rev. Lett.* **62**, 292–295.

Dahlquist, G. and Björck, A., 1974, *Numerical Methods*, Chap. 5. Prentice-Hall, Englewood Cliffs, NJ.

Ding, K. and Andersen, H. C., 1986, Molecular-dynamics simulation of amorphous germanium. *Phys. Rev.* **B34**, 6987–6991.

Erhart, P., Robrock, K. H. and Schober, H. R., 1986, Basic defects in metals, in *Physics of Radiation Effects in Crystals* (Edited by R. A. Johnson and A. N. Orlov), pp. 3–115. North-Holland, Amsterdam.

Fahey, P. M., Griffin, P. B. and Plummer, J. D., 1989, Point defects and dopant diffusion in silicon. *Rev. Mod. Phys.* **61**, 289–384.

Fortner, J. and Lannin, J. S., 1988, Radial distribution functions of amorphous silicon. *Phys. Rev.* **B39**, 5527–5530.

Gill, P. E., Murray, W. and Wright, M. H., 1981, *Practical Optimization*, pp. 102–104, 158–159. Academic Press, London.

Girifalco, L. A., 1973, *Statistical Physics of Materials*, Chap. 8. Wiley, New York.

Herring, C., 1950, Diffusional viscosity of a polycrystalline solid. *J. appl. Phys.* **21**, 437–445.

Jacucci, G. and Quirke, N., 1982, Free energy calculations for crystals, in *Computer Simulation of Solids* (Edited by C. R. A. Catlow and W. C. Mackrodt), pp. 38–52. Springer, Berlin.

Kaxiras, E. and Pandey, K. C., 1988, New classical potential for accurate simulation of atomic processes in silicon. *Phys. Rev.* **B38**, 12736–12739.

Keating, P. N., 1966, Effect of invariance requirements on the elastic strain energy of crystals with application to the diamond structure. *Phys. Rev.* **145**, 637–645.

Kirkpatrick, S., Gelatt, C. D. and Vecchi, M. P., 1983, Optimization by simulated annealing. *Science* **220**, 671–680.

Kwon, I., Biswas, R. and Soukoulis, C. M., 1991, Molecular-dynamics simulations of the stability of amorphous silicon. *Phys. Rev.* **B43**, 1859–1862.

Lannoo, M. and Bourgoin, J., 1982, *Point Defects in Semiconductors I. Theoretical Aspects*. Springer, Berlin.

LeSar, R., Najafabadi, R. and Srolovitz, D. J., 1989, Finite-temperature defect properties from free energy minimization. *Phys. Rev. Lett.* **63**, 624–627.

Lutsko, J. F., Wolf, D. and Yip, S., 1988, Molecular dynamics calculation of free energy. *J. chem. Phys.* **88**, 6525–6528.

Maroudas, D. and Brown, R. A., 1993a, Calculation of thermodynamic and transport properties of intrinsic point defects in silicon. *Phys. Rev.* **B47**, 15562–15577.

Maroudas, D. and Brown, R. A., 1993b, Atomistic calculation of the self-interstitial diffusivity in silicon. *Appl. Phys. Lett.* **62**, 172–174.

Pandey, K. C., 1986, Diffusion without vacancies or interstitials: a new concerted exchange mechanism. *Phys. Rev. Lett.* **57**, 2287–2290.

Pantelides, S. T., 1986, Defects in amorphous silicon: a new perspective. *Phys. Rev. Lett.* **57**, 2979–2982.

Pantelides, S. T., 1987, Mechanisms for peculiar low-temperature phenomena in hydrogenated amorphous silicon. *Phys. Rev. Lett.* **58**, 1344–1347.

Pantelides, S. T., 1990, Atomic diffusion processes in silicon, in *Impurities, Defects and Diffusion in Semiconductors: Bulk and Layered Structures, MRS Symposium Proceedings*, Vol. 163 (Edited by D. J. Wolford, J. Bernholc and E. E. Haller), pp. 511–521. Materials Research Society, Pittsburgh.

Pantelides, S. T., 1992, Perspectives in the past, present and future of deep centers in semiconductors, in *Deep Centers in Semiconductors: A State-of-the-Art Approach* (Edited by S. T. Pantelides), 2nd Edition, pp. 1–86. Gordon and Breach, Philadelphia.

Paul, W., Connell, G. A. N. and Temkin, R. J., 1973, Amorphous germanium I. A model for the structural and optical properties. *Adv. Phys.* **22**, 529–580.

Sabochick, M. J. and Lam, N. Q., 1990, Amorphization of

crystalline CuTi: roles of chemical disordering and non-equilibrium lattice defects. *Scripta Metal.* **24**, 565–570.
Schober, H. R., 1989, Extended interstitials in silicon and germanium. *Phys. Rev.* **B39**, 13013–13015.
Seeger, A. and Chik, P., 1968, Diffusion mechanisms and point defects in silicon and germanium. *Phys. Stat. Solidi* **29**, 455–542.
Smith, B. T., 1974, *Matrix Eigensystem Routines—EISPACK Guide.* Springer, Berlin.
Stillinger, F. H. and Weber, T. A., 1985, Computer simulation of local order in condensed phases of silicon. *Phys. Rev.* **B31**, 5262–5271.
Tan, S. I., Berry, B. S. and Crowder, B. L., 1972, Elastic and anelastic behavior of ion-implanted silicon. *Appl. Phys. Lett.* **20**, 88–90.
Tan, T. Y. and Gösele, U. M., 1985, Point defects, diffusion processes and swirl defect formation in silicon. *Appl. Phys.* **A37**, 1–17.
Tersoff, J., 1986, New empirical model for the structural properties of silicon. *Phys. Rev. Lett.* **56**, 632–635.
Tersoff, J., 1988a, New empirical approach for the structure and energy of covalent systems. *Phys. Rev.* **B37**, 6991–7000.
Tersoff, J., 1988b, Empirical interatomic potential for silicon with improved elastic properties. *Phys. Rev.* **B38**, 9902–9905.
Torres, V. J. B., Masri, P. M. and Stoneham, A. M., 1987, Two-level systems: a possible structure and its role in amorphisation. *J. Phys.* **C20**, L143–L146.
Vineyard, G. H., 1957, Frequency factors and isotope effects in solid state processes. *J. Phys. Chem. Solids* **3**, 121–128.
Watkins, G. D. and Troxell, J. R., 1980, Negative-*U* properties for point defects in silicon. *Phys. Rev. Lett.* **44**, 593–596.
Wilkinson, J. H., 1965, *The Algebraic Eigenvalue Problem*, Chap. 8. Oxford University Press, Oxford.
Wooten, F., Winer, K. and Weaire, D., 1985, Computer generation of structural models of amorphous Si and Ge. *Phys. Rev. Lett.* **54**, 1392–1395.